HHS Public Access

Author manuscript

Oncogene. Author manuscript; available in PMC 2016 January 01.

Published in final edited form as:

Oncogene. 2015 July ; 34(29): 3804–3814. doi:10.1038/onc.2014.318.

Differential roles of STAT3 in the initiation and growth of lung cancer

Jingjiao Zhou[#1,2], **Zhaoxia Qu**[#1,2], **Shapei Yan**[1,2], **Fan Sun**[1,2], **Jeffrey A. Whitsett**[4], **Steven D. Shapiro**[1,3], and **Gutian Xiao**[1,2,*]

[1]University of Pittsburgh Cancer Institute, University of Pittsburgh School of Medicine, Pittsburgh, Pennsylvania 15213, USA

[2]Department of Microbiology and Molecular Genetics, University of Pittsburgh School of Medicine, Pittsburgh, Pennsylvania 15213, USA

[3]Department of Medicine, University of Pittsburgh School of Medicine, Pittsburgh, Pennsylvania 15213, USA

[4]Divisions of Neonatology, Perinatal and Pulmonary Biology, Cincinnati Children's Hospital Medical Center, University of Cincinnati College of Medicine, Cincinnati, Ohio 45229, USA

[#] These authors contributed equally to this work.

Abstract

Signal transducer and activator of transcription 3 (STAT3) is linked to multiple cancers, including pulmonary adenocarcinoma. However, the role of STAT3 in lung cancer pathogenesis has not been determined. Using lung epithelial-specific inducible knockout strategies, we demonstrate that STAT3 plays contrasting roles in the initiation and growth of both chemically and genetically induced lung cancers. Selective deletion of lung epithelial STAT3 in mice prior to cancer induction by the smoke carcinogen, urethane, resulted in increased lung tissue damage and inflammation, K-Ras oncogenic mutations, and tumorigenesis. Deletion of lung epithelial STAT3 after establishment of lung cancer inhibited cancer cell proliferation. Simultaneous deletion of STAT3 and expression of oncogenic K-Ras in mouse lung elevated pulmonary injury, inflammation, and tumorigenesis, but reduced tumor growth. These studies indicate that STAT3 prevents lung cancer initiation by maintaining pulmonary homeostasis under oncogenic stress, whereas it facilitates lung cancer progression by promoting cancer cell growth. These studies also provide a mechanistic basis for targeting STAT3 to lung cancer therapy.

Keywords

lung cancer; lung injury; lung inflammation; lung homeostasis; Ras; STAT3

[*]Correspondence: Gutian Xiao, Hillman Cancer Center Research Pavilion, 5117 Centre Avenue, Pittsburgh, PA 15213, USA. Tel: 412-623-5410; Fax: 412-623-1415; xiaog2@upmc.edu.

Conflict of interest

The authors declare no conflict of interest.

Introduction

Lung cancer is the leading cause of cancer deaths worldwide, with a dismal 16% five-year survival rate (1). The most predominant risk factor for lung cancer is tobacco smoking, which accounts for about 87% of lung cancer cases (2). Tobacco smoke causes genetic alterations, particularly activating mutations of the K-Ras oncogene, in lung epithelium that initiates and promotes carcinogenesis (3, 4). Tobacco smoke also induces lung inflammation and damage, creating a microenvironment that facilitates oncogenic mutations and lung cancer initiation and promotion (5, 6).

Tobacco smoke contains more than sixty chemical carcinogens, and one of the well-defined and most commonly-used smoking carcinogens for cancer study is ethyl carbamate, also called urethane (2). Urethane alone is sufficient to induce K-Ras activating mutations and lung carcinogenesis in mice (7). Remarkably, murine lung cancers induced by urethane or directly driven by oncogenic K-Ras faithfully recapitulate human lung cancers, and in particular adenocarnomas associated with tobacco smoking (7). They share the same genetic and molecular changes, as well as morphology and histology. Moreover, murine lung cancers induced by urethane or K-Ras, like their human counterparts, are associated with pulmonary inflammation. Accordingly, lung carcinogenesis induced by urethane or K-Ras in mice has been well accepted and widely used as models for human lung cancers, especially those induced by smoking or associated with K-Ras mutations.

It has been well documented that K-Ras activation and inflammation induce activation of signal transducer and activator of transcription 3 (STAT3), a central regulator of numerous cellular processes, particularly cell proliferation (8, 9). STAT3 has been proposed as an oncogene, based on experiments showing that a constitutively active form of STAT3 is able to transform fibroblast or epithelia cells *in vitro* and induce epithelial carcinogenesis in mice (10-12). However, naturally occurring activating mutations of STAT3 have not been found. Moreover, both positive and negative associations between STAT3 activation and patient survival or tumor progression have been reported (13-17). Most paradoxically, loss-of-function studies indicate that STAT3 may play a positive or negative role in tumorigenesis (18-23). Thus, the role of STAT3 in tumorigenesis seems complex and requires a careful and systematic study. This is of importance, because STAT3 is a target of great interest for the prevention and treatment of lung and other cancers (24).

To dissect the role of STAT3 in lung tumorigenesis, we applied a lung epithelial-specific inducible knockout approach in both urethane- and K-Ras-induced murine lung cancer models. We find that lung epithelial STAT3 played distinct and opposing roles in the initiation and growth of lung cancer. While STAT3 is required for the maximal proliferation/progression of lung cancer cells, lung epithelial STAT3 inhibited pulmonary injury and inflammation under oncogenic stress, suppressing lung cancer initiation.

Results

Deletion of pulmonary epithelial STAT3 increased urethane-induced lung carcinogenesis

To test the functional significance of STAT3 in lung tumorigenesis, we utilized SP-C-rtTA$^{tg/-}$/(tetO)$_7$CMV-Cre$^{tg/tg}$/STAT3$^{flx/flx}$ mice, in which STAT3 could be selectively deleted in Surfactant Protein C (SP-C) positive alveolar type II epithelial cells and SP-C/Clara Cell Secretory Protein (CCSP) double positive bronchioalveolar stem cells (BASCs) after administration of doxycycline (dox). Increasing evidence suggests that alveolar type II epithelial cells and/or BASCs are the cells-of-origin of lung cancers, in particular K-Ras mutant lung cancers (25). Immunohistochemistry (IHC) and quantitative polymerase chain reaction (qPCR) analysis showed that STAT3 was efficiently deleted from alveolar type II epithelial cells and bronchiolar cells in SP-C-rtTA$^{tg/-}$/(tetO)$_7$CMV-Cre$^{tg/tg}$/STAT3$^{flx/flx}$ mice treated with dox (Figures 1a and 1b). Expression of STAT3 in neighboring cells, including alveolar type I epithelial cells and myeloid cells, was not affected (Figure 1a). Hereinafter, dox-treated SP-C-rtTA$^{tg/-}$/(tetO)$_7$CMV-Cre$^{tg/tg}$/STAT3$^{flx/flx}$ mice and their untreated littermates are referred to as STAT3$^{-/-}$ mice and STAT3$^{+/+}$ (or simply as wild type, WT) mice, respectively.

Consistent with previous findings that lung epithelial STAT3 is dispensable for lung morphogenesis and function (26, 27), STAT3$^{-/-}$ mice did not show apparent abnormalities in lung size or morphology and had normal longevity in the vivarium (Figures 1a - 1c). Notably, STAT3$^{-/-}$ mice developed significantly more lung tumors than WT mice after exposure to urethane (Figures 1c and 1d), indicating that the tumors in STAT3$^{-/-}$ mice did not originated from tumor initiating cells that escaped from Cre-mediated STAT3 deletion. In further support of this, STAT3 staining was detected in tumors in WT mice but not in STAT3$^{-/-}$ mice (Figure 1e). Histological assays also showed that urethane-induced tumors in STAT3$^{-/-}$ and WT mice were SP-C-positive and CCSP-negative, and shared similar morphology (Figure 1e, and Supplementary Figure S1). These data indicated that lung epithelial STAT3 suppressed tumor initiation in a urethane-induced lung tumorigenesis model.

Increased lung tumorigenesis in urethane-treated STAT3$^{-/-}$ mice is associated with augmented pro-tumorigenic inflammation

Recent studies indicated that pulmonary inflammation plays a critical role in the initiation and progression of lung cancer (28). To investigate the mechanisms underlying the increased lung tumorigenesis in STAT3$^{-/-}$ mice treated with urethane, we compared the pulmonary inflammation in STAT3$^{-/-}$ mice and STAT3$^{+/+}$ mice following exposure to urethane. While the expression levels of the anti-tumor cytokine interferon-gamma (IFN-γ) were comparable, concentrations of several pro-inflammatory cytokines known to promote tumor initiation and progression, including tumor necrosis factor-alpha (TNF-α), interleukin-1beta (IL-1β), and interleukin 6 (IL-6), were significantly increased in the lungs of urethane-treated STAT3$^{-/-}$ mice (Figure 2a). In addition, the immune cell-attractive chemokine CCL2 was also significantly increased in the lungs of urethane-treated STAT3$^{-/-}$ mice (Supplementary Figure S2). Accordingly, the numbers of inflammatory cells were increased in bronchioalveolar lavage fluid (BALF) from STAT3$^{-/-}$ mice treated with urethane compared

to controls (Figures 2b and 2c). Further cell type analysis indicated that lymphocytes, but not neutrophils or macrophages, were significantly increased in the BALF of urethane-treated STAT3$^{-/-}$ mice (Figures 2b-2d). These data indicated that lung epithelial STAT3 restricts urethane-induced pro-tumorigenic inflammation.

STAT3$^{-/-}$ mice are more vulnerable to urethane-induced lung damage

In association with the increased pulmonary inflammation, STAT3$^{-/-}$ mice treated with urethane had markedly exacerbated lung injury and edema, compared to controls (Figure 3, and Supplementary Figure S3). Before urethane treatment, the lung morphology and histology of STAT3$^{-/-}$ mice were not different from controls (26, 27). Exposure to urethane caused mild alveolar congestion and minor impairments of alveolar epithelial integrity in STAT3$^{+/+}$ mice, indicating mild lung injury (Figure 3a, i and ii). However, severe lung injury occurred in STAT3$^{-/-}$ mice exposed to urethane, as evidenced by marked alveolar thickening and congestion, severe loss of the integrity of the bronchiolar and alveolar epithelium, perivascular edema, and hemorrhage (Figure 3a, iii-vi). Consistently, air space enlargement, red blood cell extravasation, and accumulation of extracellular debris and protein were frequently observed in the lungs of urethane-treated STAT3$^{-/-}$ mice (Figure 3a, iii-vi). In further support of these observations, an increased protein concentration was detected in lung lavage fluid (Figure 3b). These data demonstrated that lung epithelial STAT3 protects lungs from urethane-induced pre-neoplastic injury and inflammation.

STAT3$^{-/-}$ mice are more sensitive to urethane-induced activating mutations of K-Ras

One of the important roles of local inflammation and tissue damage is to establish a microenvironment that facilitates induction of oncogenic mutations and subsequent tumor initiation and progression (5, 26). Since activating mutations of the K-Ras oncogene in lung epithelium are an early event involved in urethane-induced lung tumorigenesis in mice (29, 30), we assessed urethane-induced K-Ras mutations at codon 61, an activating mutation of K-Ras that has also identified in human lung cancers, in the lungs of urethane-treated WT and STAT3$^{-/-}$ mice (Figure 4a). The mutation rate of K-Ras in the lung type II epithelial cells of STAT3$^{-/-}$ mice was significantly higher than that in WT mice (Figure 4b), consistent with the increased incidence of lung cancer in STAT3$^{-/-}$ mice. Taken together, these data suggested that lung epithelial STAT3 prevents urethane-induced K-Ras oncogenic mutations and lung cancer initiation by maintaining pulmonary homeostasis during urethane-induced injury.

STAT3 contributes to the growth of lung cancers induced by urethane

Although STAT3$^{-/-}$ mice developed more tumor foci in the lungs than STAT3$^{+/+}$ mice after exposure to urethane, the ratio of large tumors or the average tumor size was significantly lower or smaller in STAT3$^{-/-}$ mice, respectively (Figure 5a, and Supplementary Figure S4). These data suggested that while STAT3 suppresses lung cancer initiation, it paradoxically contributes to the growth of lung cancer induced by urethane.

To further assess the role of STAT3 in the growth of lung cancers, we conditionally deleted STAT3 after urethane treatment and tumor formation. As shown in Figure 5b and Supplementary Figure S5, STAT3 was efficiently deleted at both RNA and protein levels

from urethane-induced lung tumors in mice after administration of dox. Deletion of STAT3 after tumor formation markedly reduced the size, but had no significant effect on the number of lung tumors (Figures 5c-5e), indicating that STAT3 contributes to the growth and progression of lung cancer induced by urethane. BrdU cell proliferation assays showed that $STAT3^{-/-}$ tumors had much less proliferation rate than WT tumors (Figures 5f, and Supplementary Figure S6). Mechanistic studies revealed that compared to $STAT3^{+/+}$ tumors, $STAT3^{-/-}$ tumors expressed significantly lower levels of Cyclin D1, a transcriptional target of STAT3 critical to cell proliferation (Figures 5g and 5h, and Supplementary Figure S7). These data suggested that STAT3 is required for the maximal expression of the key cell proliferation regulator Cyclin D1 and the optimal growth and progression of lung cancers induced by urethane.

STAT3 suppresses K-Ras-induced lung tumorigenesis but contributes to the growth of K-Ras mutant lung cancer

The loxP-Stop-loxP (LSL) $K\text{-}Ras^{G12D}$ genetic model of lung cancer was utilized to further assess the role of STAT3 in K-Ras-mediated pulmonary tumorigenesis. After the mutant K-Ras transgene is activated in lungs by intratracheal administration of adenoviral Cre recombinase (AdenoCre), $LSL\text{-}K\text{-}Ras^{G12D}$ mice develop lung cancers that closely resemble lung cancer in humans (31). $LSL\text{-}K\text{-}Ras^{G12D}$ mice were bred with $STAT3^{flx/flx}$ mice to generate $LSL\text{-}K\text{-}Ras^{G12D}/STAT3^{flx/flx}$ mice, in which $K\text{-}Ras^{G12D}$ expression and STAT3 deletion can be simultaneously induced in the same lung cells after AdenoCre administration. Although the administration of AdenoCre induced lung tumors in both mice, $LSL\text{-}K\text{-}Ras^{G12D}/STAT3^{-/-}$ mice developed significantly more in comparison to $LSL\text{-}K\text{-}Ras^{G12D}/STAT3^{+/+}$ mice, indicating a tumor suppressive role of STAT3 in K-Ras-driven lung tumorigenesis (Figures 6a and 6b). The deletion of STAT3 in the lung tumors of $LSL\text{-}K\text{-}Ras^{G12D}/STAT3^{-/-}$ mice were validated by both qPCR and IHC analysis (Supplementary Figure S8). Similar to our findings in the urethane model, tumors in $LSL\text{-}K\text{-}Ras^{G12D}/STAT3^{-/-}$ mice were much smaller than those in $LSL\text{-}K\text{-}Ras^{G12D}/STAT3^{+/+}$ mice (Figures 6a and 6c). Proliferation rate and expression levels of Cyclin D1 were decreased in the tumors lacking STAT3 (Figures 6d-6f, and Supplementary Figure S9).

Remarkably, in association with increased lung tumorigenesis, $LSL\text{-}K\text{-}Ras^{G12D}/STAT3^{-/-}$ mice had a significantly elevated pulmonary inflammation and injury. While the expression levels of IFN-γ were similar, increased TNF-α was detected in the lungs of $LSL\text{-}K\text{-}Ras^{G12D}/STAT3^{-/-}$ mice, compared to $LSL\text{-}K\text{-}Ras^{G12D}/STAT3^{+/+}$ mice (Figure 7a). Likewise, immune cell-attractive chemokines CCL2 and CXCL2 were significantly increased in the lungs of $LSL\text{-}K\text{-}Ras^{G12D}/STAT3^{-/-}$ mice (Figure 7b). Consistently, more inflammatory cells, particularly lymphocytes, were found the BALF from $LSL\text{-}K\text{-}Ras^{G12D}/STAT3^{-/-}$ mice (Figure 7b). Moreover, $LSL\text{-}K\text{-}Ras^{G12D}/STAT3^{-/-}$ mice showed more severe lung damage, as evidenced by enhanced alveolar thickening and congestion, loss of integrity of the alveolar capillary membrane, air space enlargement, protein leak, and red blood cell extravasation in their lungs (Figure 7c, ii-iv versus i). Thus, both the K-Ras- and urethane-induced tumor models demonstrate that STAT3 plays distinct and opposing roles in pulmonary tumorigenesis, inhibiting initiation but enhancing growth of lung cancer.

Discussion

Recent clinical studies have shown that STAT3 is activated in human lung cancers and that STAT3 activity is correlated with tumor progression, poor prognosis and short patient survival (13-15). Thus, it is of interests and importance to determine whether and how STAT3 is involved in the pathogenesis of lung cancer. These studies will not only greatly improve our understanding of lung cancer but also provide mechanistic insights into the possibility of targeting STAT3 for the treatment of the deadliest type of cancer. The present studies demonstrate, for the first time, that STAT3 plays distinct and opposing roles in the initiation as compared to progression of pulmonary adenocarcinomas.

The oncogenic role of STAT3 is supported by extensive *in vitro, in vivo* and clinical evidenc. First, constitutive activation of STAT3 has been detected in a large variety of human cancer cell lines and primary tumors, including lung cancer (13-15). Second, activation or increased expression of STAT3 has been suggested to be associated with poor patient survival and tumor progression in lung cancer and many other cancer types (13-15). Third, several major STAT3 activators, including the v-Src kinase and the IL-6 cytokine, have been shown to promote tumor initiation and progression (32, 33). Fourth, STAT3 inhibitors, including PDZ-LIM domain-containing protein 2 (PDLIM2), protein tyrosine phosphatase (PTP), protein inhibitor of activated STAT 3 (PIAS3) and suppressor of cytokine signaling 3 (SOCS3), exhibit strong tumor suppressive activities (34-41). Fifth, inhibition or knockdown of STAT3 suppresses the tumorigenicity of several types of human cancer cell lines (42, 43). Sixth, cell-specific STAT3-deficient mice are resistant to carcinogenesis, including skin carcinogenesis induced by 7,12-dimethylbenz[a]anthracene (DMBA)/12-O-tetradecanoylphorbol-13-acetate (TPA), and colon cancer initiation by azoxymethane (AOM)/dextran sulfate sodium (DSS) or adenomatosis polyposis coli Min mutant (APC^{min})(20-22). Lastly and most importantly, overexpression of constitutively active STAT3 transforms fibroblast or epithelial cells in vitro and induces epithelial carcinogenesis in mice (10-12).

In agreement with the proposed tumor-promoting functions of STAT3, we have found that genetic deletion of STAT3 from endogenous lung cancer cells in mice suppressed the growth of these malignant cells (Figures 5 and 6). Strikingly, we have also found that selective deletion of lung epithelial STAT3 increased the incidence of lung cancer induced by the chemical carcinogen urethane or oncogenic K-Ras (Figures 1 and 6). These findings suggest that STAT3 plays both promoting and suppressing roles in lung tumorigenesis. In line with the tumor suppressive functions of STAT3 in lung tumorigenesis, thyrocyte-specific deletion or inhibition of STAT3 increased thyroid tumorigenesis in a murine model of papillary thyroid carcinoma and tumorigenicity of human thyroid cancer cell lines, respectively (18). In addition, STAT3 activation in tumors has been reported to be correlated with improved patient survival, small or less aggressive tumors in several cancer types, such as breast cancer, and head and neck squamous cell carcinomas (16, 17).

Present findings demonstrate that both lung tumor-promoting and -suppressing functions of STAT3 involve its ability in promoting cell growth. Whereas STAT3 activates Cyclin D1 that likely promotes lung cancer cell proliferation (Figures 5 and 6), STAT3 suppresses lung

cancer induction by maintaining lung epithelial hemostasis under inflammatory and oncogenic stress (Figures 2, 3, 6 and 7). Loss of lung epithelial-specific STAT3 increases urethane-induced lung cell death and exacerbates the severity of lung injury induced by urethane (Figure 3, and Supplementary S3), which is associated with enhanced pulmonary inflammation, elevated K-Ras oncogenic mutations and increased lung tumor formation (Figures 2 and 4). Similarly, deletion of STAT3 from lung cells aggravates lung injury, amplifies pulmonary inflammation and augments lung tumorigenesis in mice expressing oncogenic K-Ras in their lungs (Figures 6 and 7). It seems that lung damage, inflammation, and K-Ras oncogenic activation enhance each other, and function as extrinsic and intrinsic forces to drive lung cancer initiation and progression.

Obviously, it is most likely unfeasible to completely and systemically block STAT3 activation for the therapy of lung cancer or any other types of cancers, given the physiological significance of STAT3 in humans. In this regard, no STAT3 inhibitor has been approved for use in patients, although numerous STAT3 inhibitors have been developed during the past decades (24). Our studies further suggest that even local inhibition of STAT3 within lungs may be also too toxic, because deletion of lung epithelial STAT3 alone already causes severe pulmonary injury under oncogenic and inflammatory stress (Figures 3 and 7). In addition, our studies suggest that targeting STAT3 alone is not sufficient for lung cancer therapy, because even genetic deletion of STAT3 cannot completely prevent lung tumorigenesis or induce regression of lung cancers that have already formed (Figures 5 and 6). Thus, to target STAT3 for cancer therapy, on one hand we need to lower the potential toxicity of STAT3 inhibition, and on the other hand we need to combine STAT3 inhibition with other cancer therapies for efficient clinical outcomes.

In summary, the data presented here demonstrate that lung epithelial STAT3 plays distinct and opposing roles in pulmonary tumorigenesis, suppressing initiation but enhancing growth of lung cancer. STAT3 prevents lung cancer initiation through maintaining lung hemostasis and restricting pulmonary inflammation, whereas it contributes to (although it is not absolutely required for) lung cancer growth through inducing expression of key regulators of cell proliferation. These studies not only greatly improve our understanding of the physiologic and pathogenic actions of STAT3 and the pathogenesis of lung cancer, but also provide a mechanistic basis for targeting STAT3 to treat and cure lung cancer.

Materials and Methods

Animals

SP-C-rtTA$^{tg/-}$/(tetO)7CMV-Cre$^{tg/tg}$/STAT3$^{flx/flx}$ mice and Lox-Stop-Lox (LSL) K-Ras^{G12D} mice were generated and described before (26, 27, 31). These mice were backcrossed to FVB/N wild-type mice for more than ten generations for pure FVB/N background. FVB/N STAT3$^{flx/flx}$ mice and FVB/N LSL-K-Ras mice were bred to generate FVB/N STAT3$^{flx/flx}$/LSL-K-Ras mice. All animals were housed under specific pathogen-free conditions at the Hillman Cancer Center of the University of Pittsburgh Cancer Institute. Animal experiments were approved by the Institutional Animal Care and Use Committee (IACUC) of the University of Pittsburgh.

Lung carcinogenesis

For urethane induction of lung tumors, six to eight week old SP-C-rtTA$^{tg/-}$/(tetO)7CMV-Cre$^{tg/tg}$/STAT3$^{flx/flx}$ mice pretreated with dox (STAT3$^{-/-}$) or untreated (STAT3$^{+/+}$) control mice were intraperitoneally (i.p.) injected with urethane (1 mg/g body weight) one time per week for four weeks. Alternatively, five week old mice were first injected with urethane as the same schedule, and then randomly divided into two groups: one group was administered dox, and the other one was left untreated. Three months post urethane treatment, all mice were sacrificed for lung tumor examinations. For K-Ras induction of lung tumors, six to eight week old STAT3$^{flx/flx}$/LSL-K-Ras mice and STAT3$^{+/+}$/LSL-K-Ras mice were intranasally administered 1×10^7 plaque-forming units (pfu) of Cre-expressing adenovirus (adenocre; Gene Transfer Vector Core, University of Iowa, Iowa City, IA). Three months post AdenoCre treatment, all mice were sacrificed for lung tumor examinations.

Bronchioalveolar lavage (BAL)

Mice were sacrificed, and their lungs were lavaged three times with phosphate buffered saline (PBS). The recovered BAL fluids (BALF) were centrifuged. Cells from BALF were visualized by Wright-Giemsa-staining. BALF total cell counts were determined by using a grid hemocytometer, and numbers of different leukocytes were obtained by counting at least 400 cells on Wright-Giemsa-stained cytocentrifuge slides. Supernatants of BALF were subjected to the Bicinchoninic Acid (BCA)™ protein assay (Thermo Scientific) for protein quantitation.

Lung tumor enumeration

Surface tumors in mouse lungs were counted by three blinded readers under a dissecting microscope. Tumor diameters were determined by microcalipers.

Histology and Immunohistochemistry

Mouse lungs were excised, fixed in formalin, embedded in paraffin, and cut into 4-μm-thick sections. Sections were stained with H&E, or subjected to sequential incubations with different primary antibodies and peroxidase-conjugated goat anti-rabbit secondary antibodies. The following primary antibodies were used: anti-STAT3 (Cell Signaling), anti-Cyclin D1 (Santa Cruz Biotechnology), anti-CCSP and anti-SP-C (Chemicon International).

BrdU labeling

Mice were i.p. injected with 100 mg/kg BrdU (Sigma-Aldrich) 2 hrs prior to sacrifice. Mouse lung tissue sections were stained with a BrdU in situ detection kit (BD Biosciences). More than 3000 cells per lung were counted in randomly selected fields. BrdU labeling index was calculated as the percentage of labeled cells per total cells counted as described previously (44).

Isolation of lung type II epithelial cells

The detailed protocol has been described before (45, 46). Briefly, crude lung cell suspensions were prepared by intratracheal instillation of Dispase and agarose followed by mechanical disaggregation of the lungs. Crude cell suspensions were purified by negative

selection using a biotinylated-antibody, streptavidin-coated biomagnetic particle system. Cell purities were determined by Pap staining and confirmed ultrastructurally. Purified type II cells were cultured on fibronectin-coated chamber slides and maintained for up to 5 days in DMEM with 10% fetal bovine serum (FBS).

Quantitative polymerase chain reaction (qPCR) analysis

Mouse lung tissues, BAL cells, or type II epithelial cells were subjected to RNA extraction, RNA reverse transcription and real-time PCR as described (47, 48). Genomic DNAs were also extracted from lung type II epithelial cells and used for real-time PCR. Primer pairs used for real-time PCR were: STAT3, forward 5′-GAAGACCAAGTTCATCTGTGTG-3′, reverse 5′-GGGACATCGGCAGGTCAATGGTAT-3′; IFN-γ, forward 5′-TTCTTCAGCAACAGCAAGGCGAA-3′, reverse 5′-TGAATGCTTGGCGCTGGACCTG-3′; TNF-α, forward 5′-GATGAGAAGTTCCCAAATGGC-3′, reverse 5′-ACTTGGTGGTTTGCTACGACG-3′; IL-1β, forward 5′-CAACCAACAAGTGATATTCTCCATG-3′, reverse 5′-GATCCACACTCTCCAGCTGCA-3′; IL-6, forward 5′-AGACAAAGCCAGAGTCCTTCAGAGA-3′, reverse 5′-TAGCCACTCCTTCTGTGACTCCAGC-3′; CCL2, forward 5′-GCTGTTCACAGTTGCCGGCTG-3′, reverse 5′-GGGCGTTAACTGCATCTGGCT-3′; CXCL2, forward 5′-ACCAACCACCAGGCTACAG-3′, reverse 5′-GCGTCACACTCAAGCTCT-3′; Cyclin D1, forward 5-CAAAATGCCAGAGGCGGATG-3′, reverse 5′-CATGGAGGGTGGGTTGGAAA-3′; β-actin, forward 5′-ACCCGCGAGCACAGCTTCTTTG-3′, reverse 5′-CTTTGCACATGCCGGAGCCGTTG-3′.

K-Ras sequencing

The exon 2 of the K-Ras gene was amplified by PCR using AccuPrime Pfx polymerase (Invitrogen) and the following primers: forward 5′-TACAGGAAACAAGTAGTAATTGATGGAGAA-3′; reverse 5′-ATAATGGTGAATATCTTCAAATGATTTAGT-3′. The PCR products were then directly used for DNA sequencing. The mutation frequencies of K-Ras in type II lung epithelial cells were determined by the ratios of the area of the mutated nucleotide versus that of wild type nucleotide of K-Ras in the sequencing map.

Statistical Analysis

Data were reported as mean ± standard deviation (SD). The Student’s t test (two tailed) was used to assess significance of differences between two groups, and p values < 0.05 and 0.01 were considered statistically significant and highly statistically significant, respectively (36, 37).

Supplementary Material

Refer to Web version on PubMed Central for supplementary material.

Acknowledgments

This study was supported in part by the National Institute of Health (NIH)/National Cancer Institute (NCI) grants R01 CA172090, R21 CA175252, P30 CA047904, as well as the American Lung Association (ALA) Lung Cancer Discovery Award and American Cancer Society (ACS) Fellowship RSG-06-066-01-MGO.

References

1. Siegel R, Naishadham D, Jemal A. Cancer statistics, 2013. CA Cancer J Clin. 2013; 63:11–30. [PubMed: 23335087]
2. Hecht SS. Cigarette smoking and lung cancer: chemical mechanisms and approaches to prevention. Lancet Oncol. 2002; 3:461–469. [PubMed: 12147432]
3. Herbst RS, Heymach JV, Lippman SM. Lung cancer. N Engl J Med. 2008; 359:1367–1380. [PubMed: 18815398]
4. Riely GJ, Marks J, Pao W. KRAS mutations in non-small cell lung cancer. Proc Am Thorac Soc. 2009; 6:201–205. [PubMed: 19349489]
5. Smith CJ, Perfetti TA, King JA. Perspectives on pulmonary inflammation and lung cancer risk in cigarette smokers. Inhal Toxicol. 2006; 18:667–677. [PubMed: 16864557]
6. Hussain SP, Hofseth LJ, Harris CC. Radical causes of cancer. Nat Rev Cancer. 2003; 3:276–285. [PubMed: 12671666]
7. Tuveson DA, Jacks T. Modeling human lung cancer in mice: similarities and shortcomings. Oncogene. 1999; 18:5318–5324. [PubMed: 10498884]
8. Yu H, Pardoll D, Jove R. STATs in cancer inflammation and immunity: a leading role for STAT3. Nat Rev Cancer. 2009; 9:798–809. [PubMed: 19851315]
9. Li N, Grivennikov SI, Karin M. The unholy trinity: inflammation, cytokines, and STAT3 shape the cancer microenvironment. Cancer Cell. 2011; 19:429–431. [PubMed: 21481782]
10. Bromberg JF, Wrzeszczynska MH, Devgan G, Zhao Y, Pestell RG, Albanese C, et al. Stat3 as an oncogene. Cell. 1999; 98:295–303. [PubMed: 10458605]
11. Azare J, Leslie K, Al-Ahmadie H, Gerald W, Weinreb PH, Violette SM, et al. Constitutively activated Stat3 induces tumorigenesis and enhances cell motility of prostate epithelial cells through integrin beta 6. Mol Cell Biol. 2007; 27:4444–4453. [PubMed: 17438134]
12. Li Y, Du H, Qin Y, Roberts J, Cummings OW, Yan C. Activation of the signal transducers and activators of the transcription 3 pathway in alveolar epithelial cells induces inflammation and adenocarcinomas in mouse lung. Cancer Res. 2007; 67:8494–8503. [PubMed: 17875688]
13. Mostertz W, Stevenson M, Acharya C, Chan I, Walters K, Lamlertthon W, et al. Age- and sex-specific genomic profiles in non-small cell lung cancer. JAMA. 2010; 303:535–543. [PubMed: 20145230]
14. Jiang R, Jin Z, Liu Z, Sun L, Wang L, Li K. Correlation of activated STAT3 expression with clinicopathologic features in lung adenocarcinoma and squamous cell carcinoma. Mol Diagn Ther. 2011; 15:347–352. [PubMed: 22208386]
15. Ai T, Wang Z, Zhang M, Zhang L, Wang N, Li W, et al. Expression and prognostic relevance of STAT3 and cyclin D1 in non-small cell lung cancer. Int J Biol Markers. 2012; 27:e132–138. [PubMed: 22467101]
16. Dolled-Filhart M, Camp RL, Kowalski DP, Smith BL, Rimm DL. Tissue microarray analysis of signal transducers and activators of transcription 3 (Stat3) and phospho-Stat3 (Tyr705) in node-negative breast cancer shows nuclear localization is associated with a better prognosis. Clin Cancer Res. 2003; 9:594–600. [PubMed: 12576423]
17. Pectasides E, Egloff AM, Sasaki C, Kountourakis P, Burtness B, Fountzilas G, et al. Nuclear localization of signal transducer and activator of transcription 3 in head and neck squamous cell carcinoma is associated with a better prognosis. Clin Cancer Res. 2010; 16:2427–2434. [PubMed: 20371693]
18. Couto JP, Daly L, Almeida A, Knauf JA, Fagin JA, Sobrinho-Simões M, et al. STAT3 negatively regulates thyroid tumorigenesis. Proc Natl Acad Sci USA. 2012; 109:E2361–2370. [PubMed: 22891351]

19. de la Iglesia N, Konopka G, Puram SV, Chan JA, Bachoo RM, You MJ, et al. Identification of a PTEN-regulated STAT3 brain tumor suppressor pathway. Genes Dev. 2008; 22:449–462. [PubMed: 18258752]
20. Musteanu M, Blaas L, Mair M, Schlederer M, Bilban M, Tauber S, et al. Stat3 is a negative regulator of intestinal tumor progression in Apc(Min) mice. Gastroenterology. 2010; 138:1003–1011. [PubMed: 19962983]
21. Chan KS, Sano S, Kiguchi K, Anders J, Komazawa N, Takeda J, et al. Disruption of Stat3 reveals a critical role in both the initiation and the promotion stages of epithelial carcinogenesis. J Clin Invest. 2004; 114:720–728. [PubMed: 15343391]
22. Grivennikov S, Karin E, Terzic J, Mucida D, Yu GY, Vallabhapurapu S, et al. IL-6 and Stat3 are required for survival of intestinal epithelial cells and development of colitis-associated cancer. Cancer Cell. 2009; 15:103–113. [PubMed: 19185845]
23. Ihara S, Kida H, Arase H, Tripathi LP, Chen YA, Kimura T, et al. Inhibitory roles of signal transducer and activator of transcription 3 in antitumor immunity during carcinogen-induced lung tumorigenesis. Cancer Res. 2012; 72:2990–2999. [PubMed: 22659452]
24. Peyser ND, Grandis JR. Critical analysis of the potential for targeting STAT3 in human malignancy. Onco Targets Ther. 2013; 6:999–1010. [PubMed: 23935373]
25. Xu X, Rock JR, Lu Y, Futtner C, Schwab B, Guinney J, et al. Evidence for type II cells as cells of origin of K-Ras-induced distal lung adenocarcinoma. Proc Natl Acad Sci USA. 2012; 109:4910–4915. [PubMed: 22411819]
26. Hokuto I, Ikegami M, Yoshida M, Takeda K, Akira S, Perl AK, et al. Stat-3 is required for pulmonary homeostasis during hyperoxia. J Clin Invest. 2004; 113:28–37. [PubMed: 14702106]
27. Matsuzaki Y, Xu Y, Ikegami M, Besnard V, Park KS, Hull WM, et al. Stat3 is required for cytoprotection of the respiratory epithelium during adenoviral infection. J Immunol. 2006; 177:527–537. [PubMed: 16785550]
28. Dougan M, Li D, Neuberg D, Mihm M, Googe P, Wong KK, et al. A dual role for the immune response in a mouse model of inflammation-associated lung cancer. J Clin Invest. 2011; 121:2436–2446. [PubMed: 21537082]
29. Ichikawa T, Yano Y, Uchida M, Otani S, Hagiwara K, Yano T. The activation of K-ras gene at an early stage of lung tumorigenesis in mice. Cancer Lett. 1996; 107:165–170. [PubMed: 8947508]
30. Wang X, Witschi H. Mutations of the Ki-ras protooncogene in 3-methylcholanthrene and urethan-induced and butylated hydroxytoluene-promoted lung tumors of strain A/J and SWR mice. Cancer Lett. 1995; 91:33–39. [PubMed: 7750092]
31. Jackson EL, Willis N, Mercer K, Bronson RT, Crowley D, Montoya R, et al. Analysis of lung tumor initiation and progression using conditional expression of oncogenic K-ras. Genes Dev. 2001; 15:3243–3248. [PubMed: 11751630]
32. Yu CL, Meyer DJ, Campbell GS, Larner AC, Carter-Su C, Schwartz J, et al. Enhanced DNA-binding activity of a Stat3-related protein in cells transformed by the Src oncoprotein. Science. 1995; 269:81–83. [PubMed: 7541555]
33. Chang Q, Bournazou E, Sansone P, Berishaj M, Gao SP, Daly L, et al. The IL-6/JAK/Stat3 feed-forward loop drives tumorigenesis and metastasis. Neoplasia. 2013; 15:848–862. [PubMed: 23814496]
34. Qu Z, Fu J, Ma H, Zhou J, Jin M, Mapara MY, et al. PDLIM2 restricts Th1 and Th17 differentiation and prevents autoimmune disease. Cell Biosci. 2012; 2:23. [PubMed: 22731402]
35. Yan P, Fu J, Qu Z, Li S, Tanaka T, Grusby MJ, Xiao G. PDLIM2 suppresses HTLV-I Tax-mediated tumorigenesis by targeting Tax into the nuclear matrix for proteasomal degradation. Blood. 2009; 113:4370–4380. [PubMed: 19131544]
36. Qu Z, Fu J, Yan P, Hu J, Cheng SY, Xiao G. Epigenetic repression of PDLIM2: implications for the biology and treatment of breast cancer. J Biol Chem. 2010; 285:11786–11792. [PubMed: 20185823]
37. Qu Z, Yan P, Fu J, Jiang J, Grusby MJ, Smithgall TE, et al. DNA methylation-dependent repression of PDLIM2 in colon cancer and its role as a potential therapeutic target. Cancer Res. 2010; 70:1766–1772. [PubMed: 20145149]

38. Yan P, Qu Z, Ishikawa C, Mori N, Xiao G. Human T-cell leukemia virus type I-mediated repression of PDZ-LIM domain-containing protein 2 involves DNA methylation but independent of the viral oncoprotein tax. Neoplasia. 2009; 11:1036–1041. [PubMed: 19794962]
39. Fu J, Yan P, Li S, Qu Z, Xiao G. Molecular determinants of PDLIM2 in suppressing HTLV-I Tax-mediated tumorigenesis. Onocogene. 2010; 29:6499–6507.
40. Zhang X, Guo A, Yu J, Possemato A, Chen Y, Zheng W, et al. Identification of STAT3 as a substrate of receptor protein tyrosine phosphatase T. Proc Natl Acad Sci USA. 2007; 104:4060–4064. [PubMed: 17360477]
41. Brantley EC, Nabors LB, Gillespie GY, Choi YH, Palmer CA, Harrison K, et al. Loss of protein inhibitors of activated STAT-3 expression in glioblastoma multiforme tumors: implications for STAT-3 activation and gene expression. Clin Cancer Res. 2008; 14:4694–4704. [PubMed: 18676737]
42. Sen M, Thomas SM, Kim S, Yeh JI, Ferris RL, Johnson JT, et al. First-in-human trial of a STAT3 decoy oligonucleotide in head and neck tumors: implications for cancer therapy. Cancer Discov. 2012; 2:694–705. [PubMed: 22719020]
43. Pan Y, Zhou F, Zhang R, Claret FX. Stat3 inhibitor Stattic exhibits potent antitumor activity and induces chemo- and radio-sensitivity in nasopharyngeal carcinoma. PLoS One. 2013; 8:e54565. [PubMed: 23382914]
44. Qu Z, Sun D, Young W. Lithium promotes neural precursor cell proliferation: evidence for the involvement of the non-canonical GSK-3β-NF-AT signaling. Cell Biosci. 2011; 1:18. [PubMed: 21711903]
45. Rice WR, Conkright JJ, Na CL, Ikegami M, Shannon JM, Weaver TE. Maintenance of the mouse type II cell phenotype in vitro. Am J Physiol Lung Cell Mol Physiol. 2002; 283:L256–264. [PubMed: 12114186]
46. Corti M, Brody AR, Harrison JH. Isolation and primary culture of murine alveolar type II cells. Am *J Respir Cell Mol Biol*. 1996; 14:309–315. [PubMed: 8600933]
47. Qing G, Qu Z, Xiao G. Endoproteolytic processing of C-terminally truncated NF-κB2 precursors at κB-containing promoters. Proc Natl Acad Sci USA. 2007; 104:5324–5329. [PubMed: 17363471]
48. Qing G, Qu Z, Xiao G. Stabilization of basally translated NF-κB-inducing kinase (NIK) protein functions as a molecular switch of processing of NF-κB2 p100. J Biol Chem. 2005; 280:40578–40582. [PubMed: 16223731]

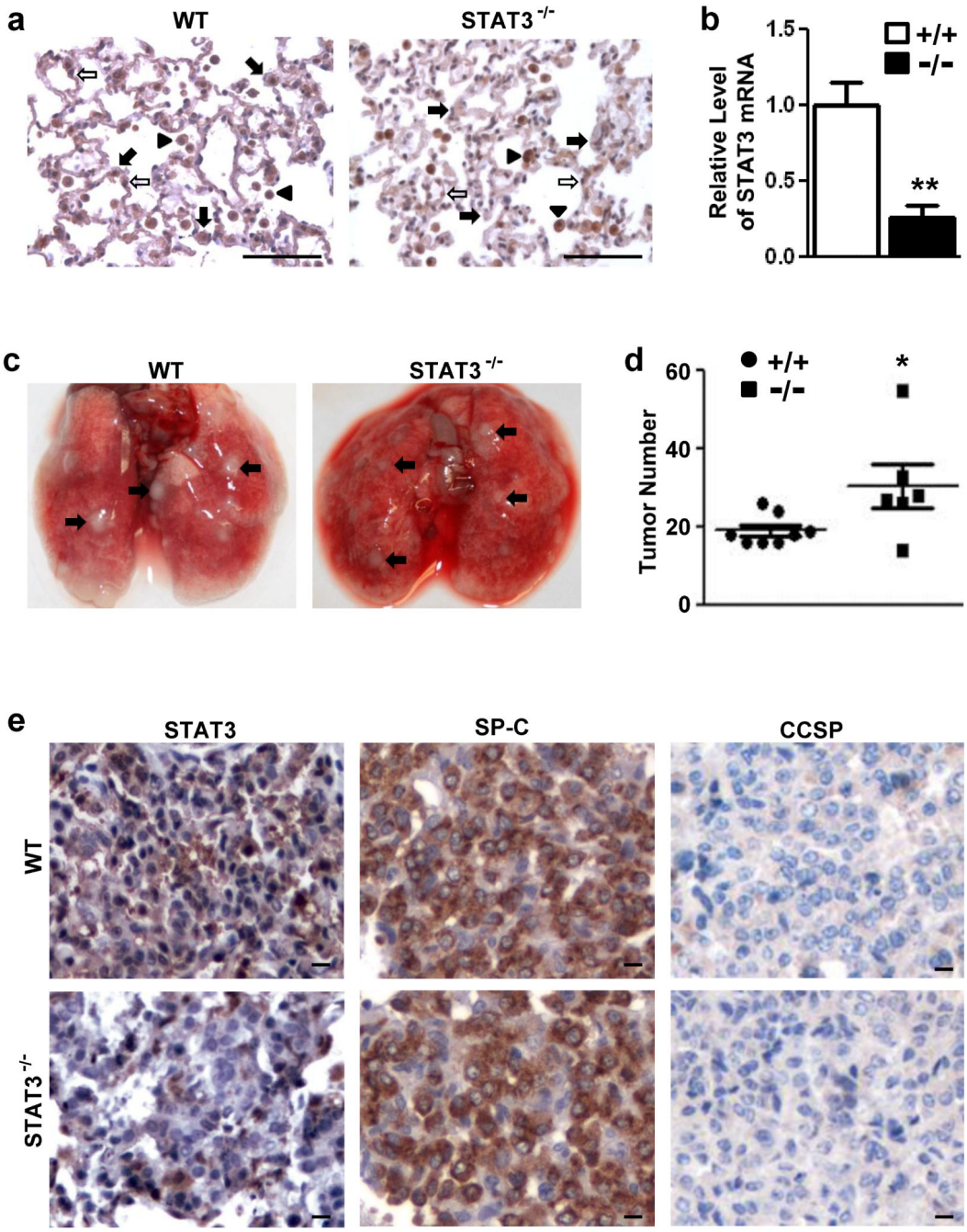

Figure 1.

Lung epithelial-specific STAT3 deficient ($STAT3^{-/-}$) mice are more susceptible to urethane-induced lung tumorigenesis than wild type (WT) mice. (**a**) Lung tissues from $STAT3^{-/-}$ mice and WT mice were immunostained for STAT3. Representative alveolar type II epithelia cells, type I epithelia cells and macrophage cells are indicated by the filled arrows, open arrows and arrowheads, respectively. Scale bar: 50 μm. (**b**) Alveolar type II cells from $STAT3^{-/-}$ mice and WT mice were analyzed by real-time RT-PCR for the relative expression levels of STAT3 mRNA. Data were normalized to β-actin and presented

as means ± standard deviation (SD) (n ≥ 5; **, $p < 0.01$). (**c**) Lung and tumor appearance in urethane-treated STAT3$^{-/-}$ mice and WT mice. Representative tumors are indicated by arrows. (**d**) Lung tumor multiplicities in urethane-treated STAT3$^{\Delta/\Delta}$ mice and WT mice are shown. Data are the mean ± SD (n ≥ 6; *, $p < 0.05$). (**e**) Representative immunohistochemical analysis of STAT3, SP-C and CCSP in lung tumors from urethane-treated STAT3$^{-/-}$ mice and WT mice. Scale bar: 10 μm.

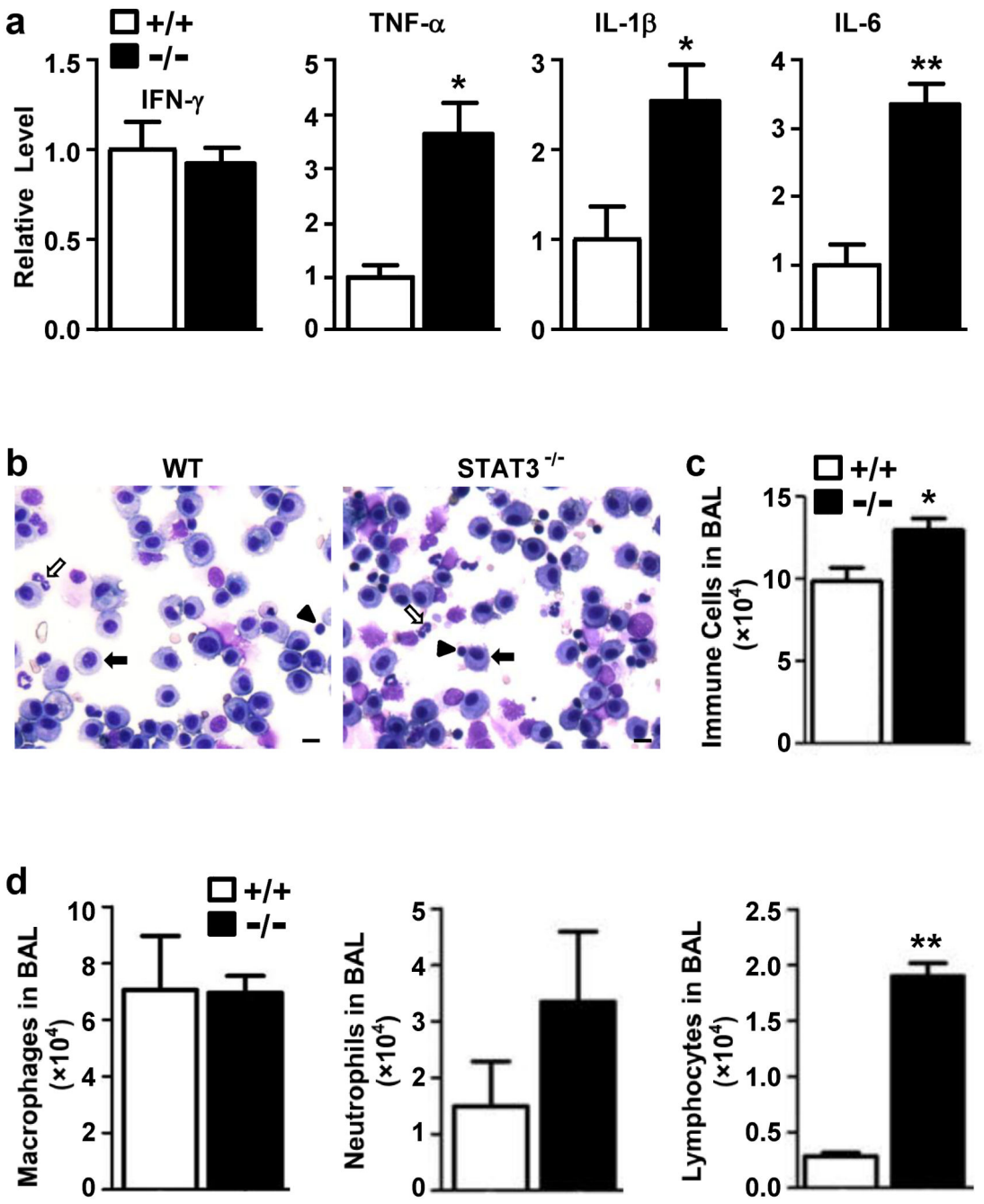

Figure 2.

STAT3$^{-/-}$ mice are more susceptible to urethane-induced pulmonary inflammation than WT mice. (**a**) Relative expression levels of cytokines IFN-γ, TNF-α, IL-1β, and IL-6 in lungs of urethane-treated STAT3$^{-/-}$ mice and WT mice. Data are the mean ± SD (n ≥ 5; *, $p < 0.05$; **, $p < 0.01$). (**b**) Hema 3 staining of BAL cells from urethane-treated STAT3$^{-/-}$ mice and WT mice on cytocentrifuge slides. Representative macrophages and neutrophils and lymphocytes were indicated by the filled arrows, open arrows and arrowheads, respectively. Scale bar: 10 μm. (**c**) Total immune cell numbers in BALF from urethane-treated STAT3$^{-/-}$

mice and WT mice. Data are the mean ± SD (n ≥ 5; *, $p < 0.05$). (**d**) Cell numbers of macrophages, neutrophils and lymphocytes in BALF from urethane-treated STAT3$^{-/-}$ mice and WT mice. Data are the mean ± SD (n ≥ 5; **, $p < 0.01$).

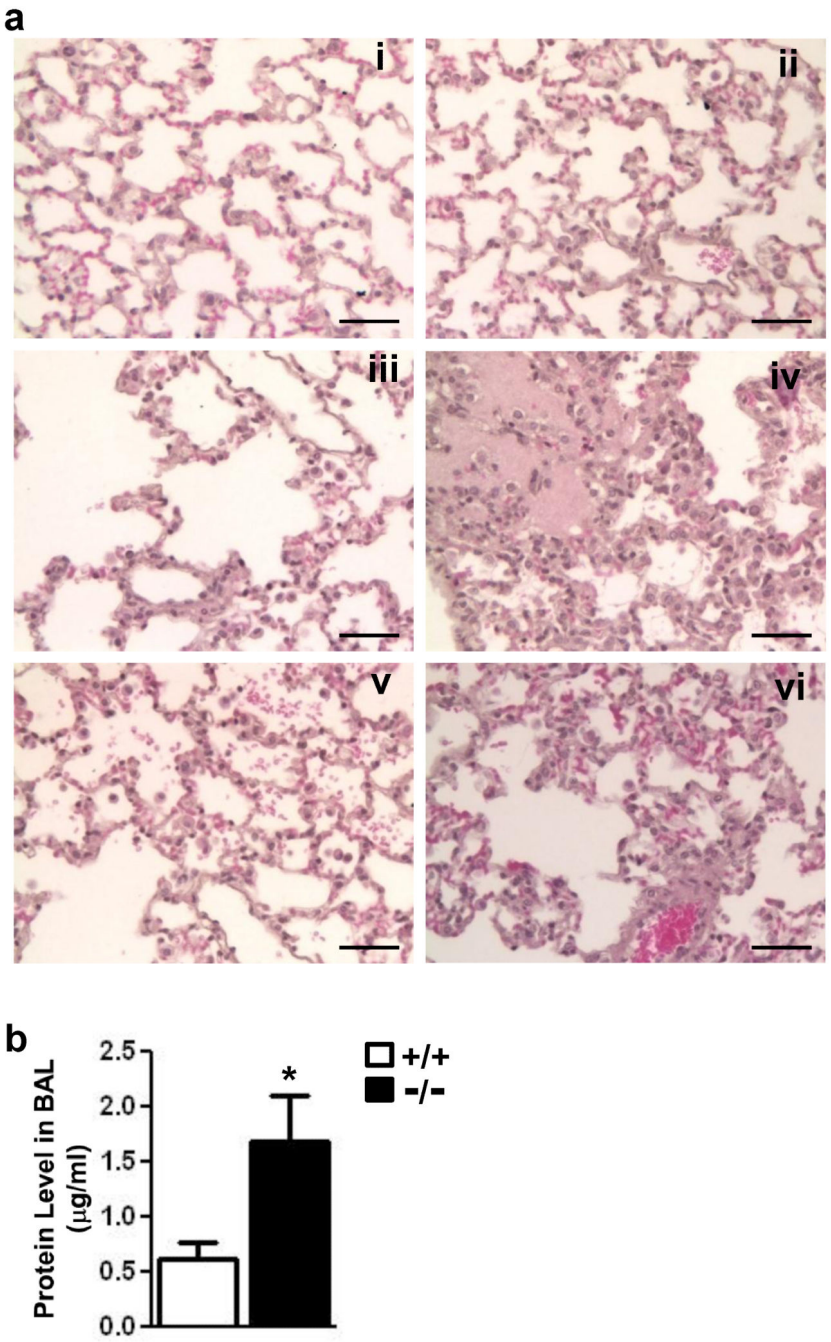

Figure 3.

STAT3$^{-/-}$ mice are susceptible to urethane-induced lung injury. (**a**) Histological analysis showing severe lung injury in urethane-treated STAT3$^{-/-}$ mice. Minor histologic changes in lungs from STAT3$^{+/+}$ mice after urethane exposure (**i** and **ii**). Severe epithelial cell death, protein leak, thickened alveoli, perivascular edema and hemorrhage in lungs from STAT3$^{-/-}$ mice after urethane exposure (**iii-vi**). Scale bar: 50 μm. (**b**) BAC™ protein assay showing high protein concentration in BALF from urethane-treated STAT3$^{-/-}$ mice. Data are the mean ± SD (n = 3; *, $p < 0.05$).

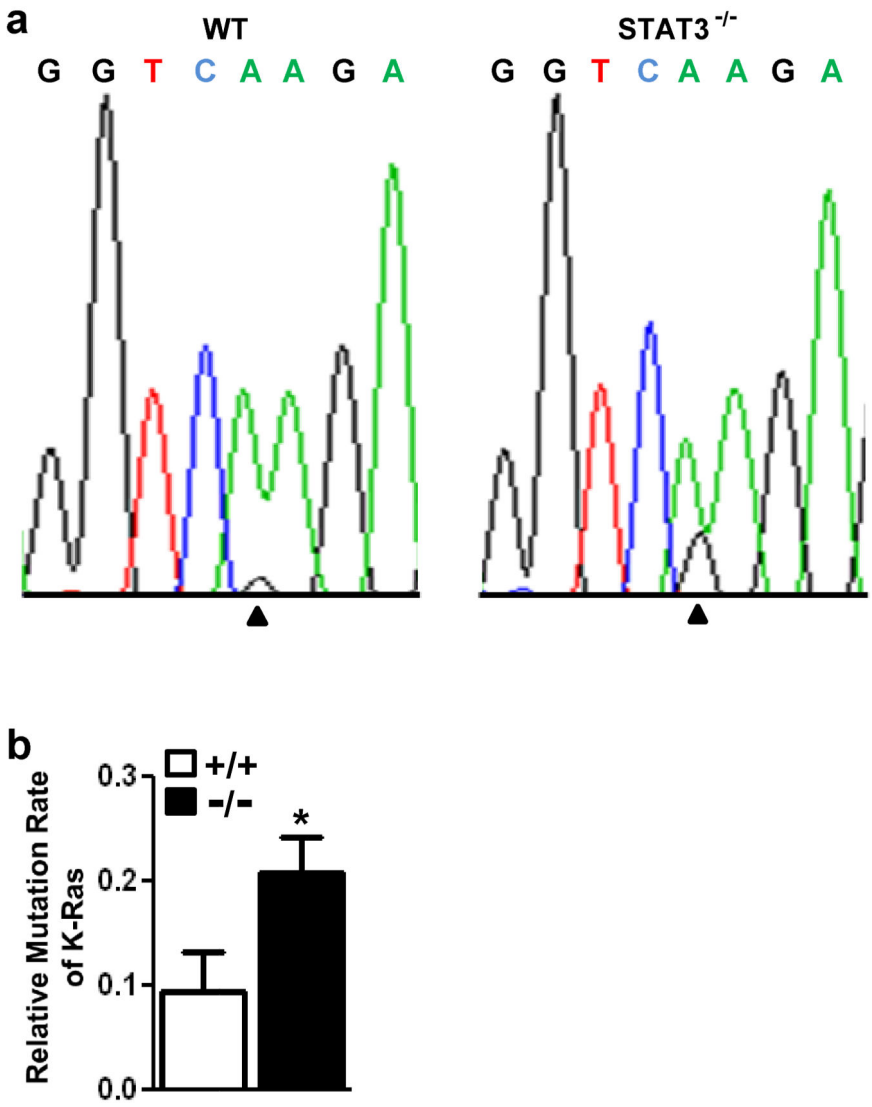

Figure 4.

STAT3$^{-/-}$ mice are more susceptible to urethane-induced K-Ras activating mutations than WT mice. (**a**) Representative sequencing analysis of K-Ras mutations at codon 61 in the lung cells of urethane-treated STAT3$^{-/-}$ mice and WT mice. The mutated nucleotides are indicated be arrowheads. (**b**) Comparison of K-Ras mutation frequency in the lungs of STAT3$^{-/-}$ mice and STAT3$^{+/+}$ mice. Data are the mean ± SD (n = 4; *, $p < 0.05$)

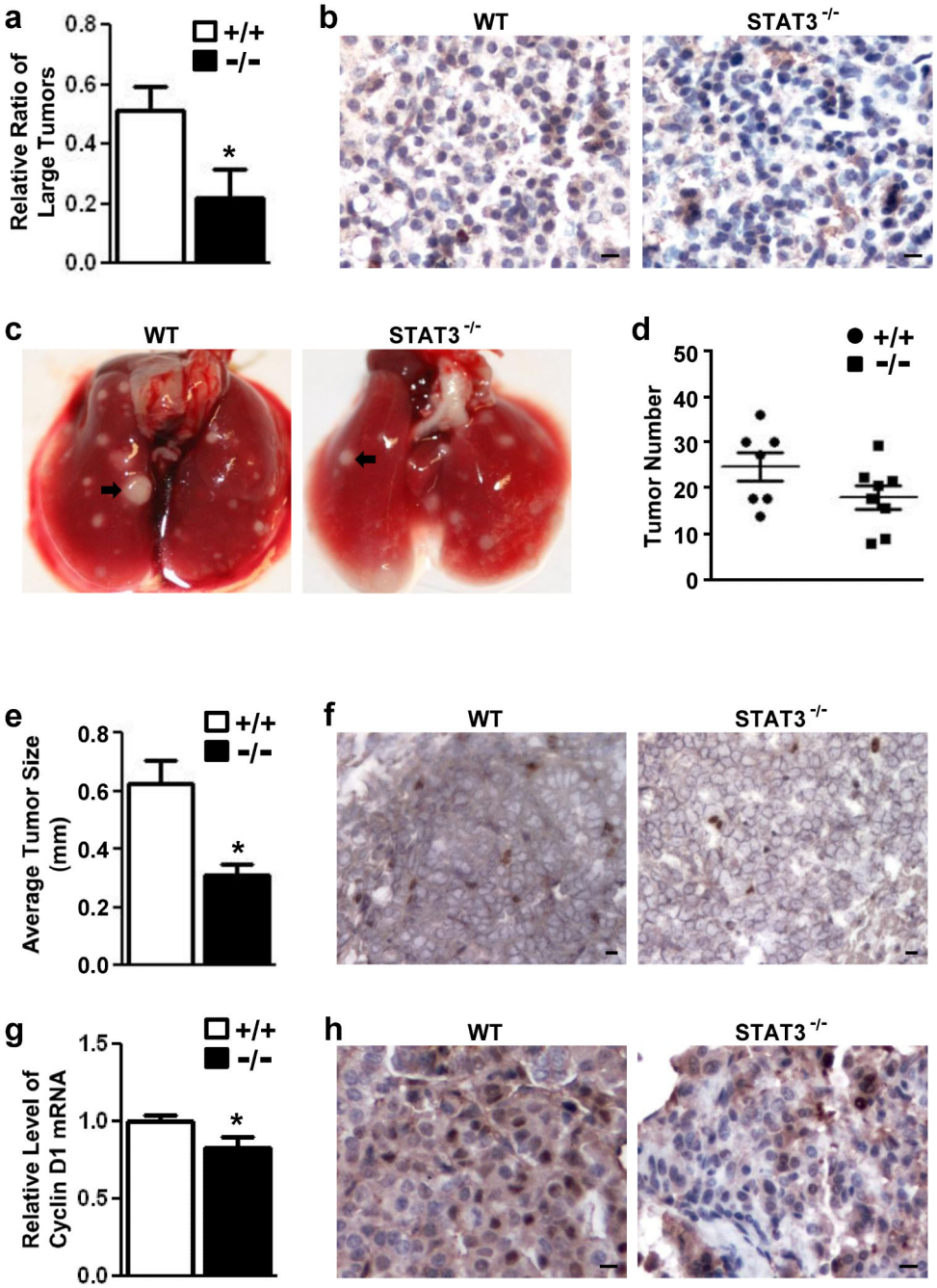

Figure 5.

STAT3 is involved in the growth of lung cancer induced by urethane. (**a**) Percentiles of large lung tumors among total tumors in urethane-treated $STAT3^{-/-}$ mice and $STAT3^{+/+}$ mice. Tumors with a diameter equal to or bigger than 0.5 mm are defined as large tumors. Data are the mean ± SD ($n \geq 6$; *, $p < 0.05$). (**b**) Representative immunohistochemical analysis showing STAT3 deletions from established lung tumors in urethane-treated mice. Scale bar: 10 μm. (**c**) Lung and tumor appearance in mice in which STAT3 was intact or deleted from tumors after tumor establishment. Representative tumors are indicated by

arrows. (**d**) Deletion of STAT3 after lung tumor establishment had no significant effect on tumor number. Data are the mean ± SD (n ≥ 7). (**e**) Deletion of STAT3 after lung tumor establishment significantly decreased tumor size. Data are the mean ± SD (n ≥ 7; *, $p < 0.05$). (**f**) BrdU labeling showing decreased proliferation of $STAT3^{-/-}$ lung tumor cells. Scale bar: 10 μm. (**g**) qPCR analysis showing lower expression levels of Cyclin D1 RNA in $STAT3^{-/-}$ lung tumors. Data are the mean ± SD (n ≥ 7; *, $p < 0.05$). (**h**) Immunohistochemical analysis showing lower expression levels of Cyclin D1 protein in $STAT3^{-/-}$ lung tumors. Scale bar: 10 μm.

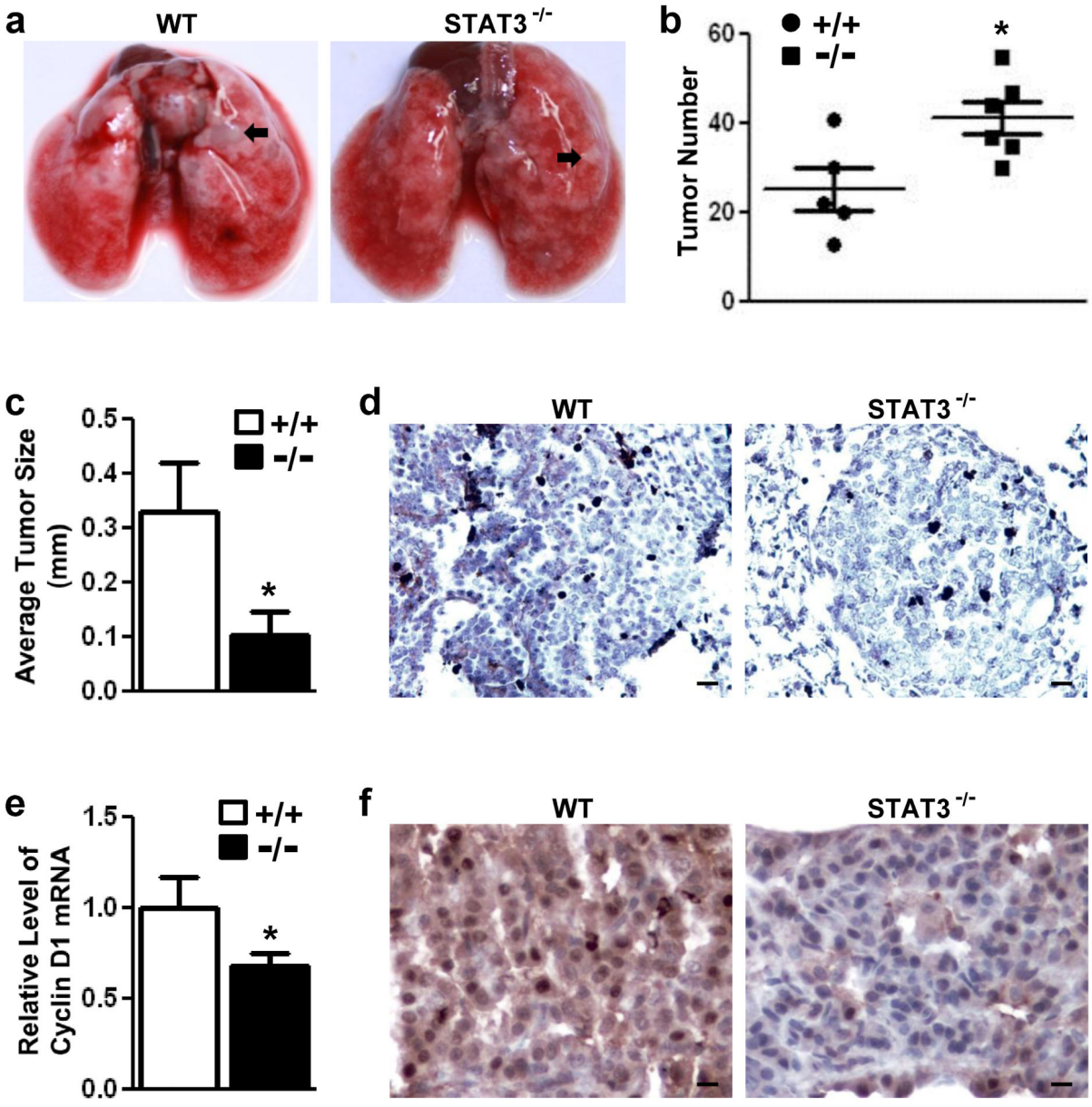

Figure 6.

STAT3 deletion increases K-Ras-driven lung tumorigenesis but decreases K-Ras-driven lung cancer growth. (**a**) Lung and tumor appearance in K-Ras^{G12D}/STAT3$^{-/-}$ mice and K-Ras^{G12D}/STAT3$^{+/+}$ mice. Representative tumors are indicated by arrows. (**b**) Lung tumor multiplicities in K-Ras^{G12D}/STAT3$^{-/-}$ mice and K-Ras^{G12D}/STAT3$^{+/+}$ mice. Data are the mean ± SD (n ≥ 5; *, $p < 0.05$). (**c**) Average size of lung tumors in K-Ras^{G12D}/STAT3$^{-/-}$ mice and K-Ras^{G12D}/STAT3$^{+/+}$ mice. Data are the mean ± SD (n ≥ 5; *, $p < 0.05$). (**d**) BrdU labeling was decreased in STAT3$^{-/-}$ lung tumors. (**e**) qPCR analysis showing decreased Cyclin D1 mRNA in K-Ras^{G12D}/STAT3$^{-/-}$ lung tumors. Data are the mean ± SD (n ≥ 5; *, $p < 0.05$). Scale bar: 50 μm. (**f**) Immunohistochemical analysis showing decreased Cyclin D1 protein in STAT3$^{-/-}$ lung tumors. Scale bar: 10 μm.

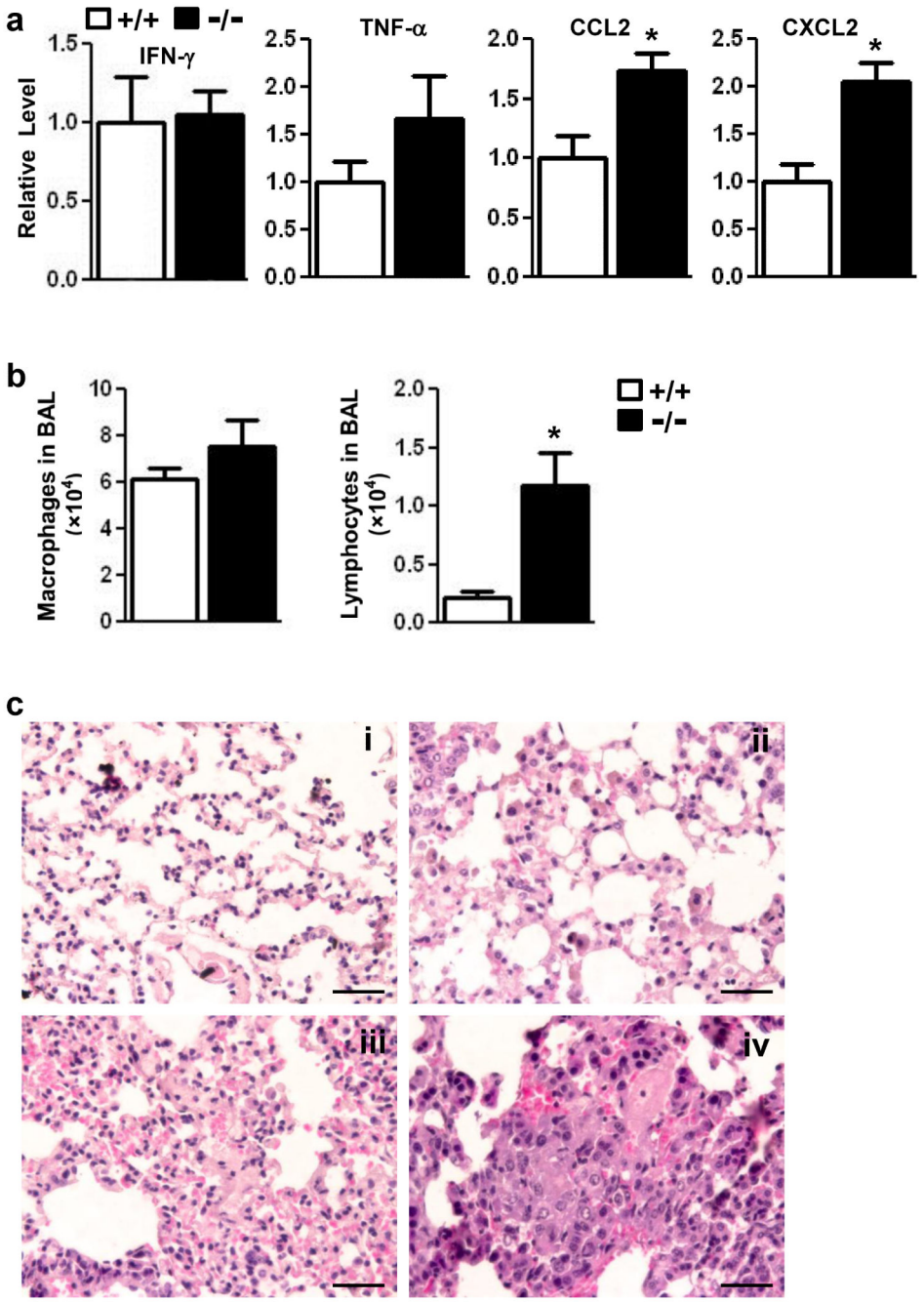

Figure 7.

Increased lung tumorigenesis in K-Ras^{G12D}/ STAT3$^{-/-}$ mice is associated with increased pulmonary inflammation and damage. (**a**) Relative expression levels of cytokines IFN-γ, TNF-α, CCL2 and CXCL2 in lungs of K-Ras^{G12D}/STAT3$^{-/-}$ mice and K-Ras^{G12D}/STAT3$^{+/+}$ mice. Data are the mean ± SD (n ≥ 5; *, $p < 0.05$). (**b**) Total numbers of inflammatory cells and cell numbers of macrophages and lymphocytes in BALF from K-Ras^{G12D}/STAT3$^{-/-}$ mice and K-Ras^{G12D}/STAT3$^{+/+}$ mice. Data are the mean ± SD (n ≥ 3; *, $p < 0.05$). (**c**) Histological analysis showing increased lung injury in K-Ras^{G12D}/STAT3$^{-/-}$

mice. Lung histology of K-Ras^{G12D}/STAT3$^{+/+}$ mice (**i**) and K-Ras^{G12D}/STAT3$^{-/-}$ mice (**ii-iv**). Scale bar: 50 μm.